

# Fully-Scalable 2D THz Radiating Array: A 42-Element Source in 130-nm SiGe with 80- $\mu$ W Total Radiated Power at 1.01 THz

Zhi Hu and Ruonan Han

Dept. of Electrical Engineering and Computer Science, Microsystem Technology Laboratories  
Massachusetts Institute of Technology

**Abstract**—This paper presents a 1-THz radiating array using IHP 130-nm SiGe process. It is based on a highly-scalable 2D structure that uses a square grid of slots to simultaneously (1) maximize and synchronize the fundamental oscillation ( $f_0=250$  GHz) and 4<sup>th</sup>-harmonic generation ( $4f_0=1$  THz) of a large array of transistors, (2) synthesize standing-wave patterns with near-field cancellation at  $f_0$ ,  $2f_0$  and  $3f_0$  and efficient radiation at  $4f_0$ . The compact design enables implementation of 42 coherent radiators on a 1-mm<sup>2</sup> area. The chip consumes 1.1-W DC power and generates 80- $\mu$ W total radiated power with 13-dBm EIRP.

**Index Terms**—THz source, scalable radiating array, SiGe

## I. INTRODUCTION

Pushing the radiation frequency of solid-state sources towards the center of the terahertz gap at around 1 THz enables new opportunities in ro-vibrational spectroscopy for biomaterials, ultra-high-resolution imaging, sub- $\mu$ m vibrometry, etc. However, the radiated power produced by previous silicon sources is still low. In [1] and [2], active multipliers in SiGe generate an effective isotropic radiated power (EIRP) of -37 dBm at 1 THz and -17 dBm at 0.82 THz, respectively. Using MOS varactors, a 1.33-THz CMOS passive multiplier [3] generates an EIRP of -13 dBm and a total radiated power of 6  $\mu$ W. Large-scale 2D quasi-optical power combining is expected to reach a power level well beyond the current state-of-the-arts. However, there are two major challenges:

1) : The radiator units should be self-sustaining and phase/frequency synchronized. Coupled-oscillator array is an ideal choice, but optimal unit pitch (to minimize sidelobes in the radiation pattern)  $\lambda_{f_{rad}}/2$  at 1 THz in this process is only  $\sim 90\mu m$ , making it very difficult to fit oscillator, antenna, filters, etc. into a single unit, especially for high-order harmonic radiation when  $\lambda_{f_{osc}} \gg \lambda_{f_{rad}}$ .

2) : At such high frequency, where passive components are very lossy, transistors still need to oscillate near  $f_{max}$ . To maximize efficiency, optimal device conditions and terminations at all harmonics should be met with ultra-compact while multi-functional structures.

This paper reports a 1-THz radiating array in SiGe that fully addresses these challenges. It achieves 13-dBm EIRP and 80- $\mu$ W total radiated power—the highest in all Si-based coherent radiators operating above 0.5 THz.

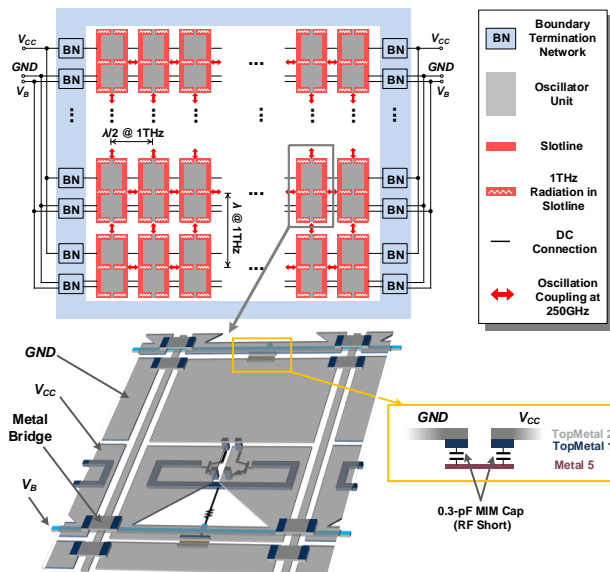


Fig. 1. Topology of the 1-THz radiating array and 3D view of a single unit.

## II. OVERVIEW OF THE RADIATOR ARCHITECTURE

The radiator architecture is shown in Fig. 1. It is an array of oscillator units featuring a rectangular loop of metal slots at the boundary and a horizontal slot at its center. Each unit, consisting of two top-metal square patches, contains a 250-GHz ( $f_0$ ) oscillating SiGe-HBT pair which delivers fundamental and harmonic standing waves to the slots. In Section III, we show that (1) only the radiation at  $4f_0$  (1 THz) is generated, by all horizontal slots, and (2) in-phase oscillation/radiation are achieved by abutting the units vertically and horizontally. The dimension of each square patch in the oscillator unit is  $\lambda_{4f_0}/4$ , which permits maximum sidelobe radiation suppression. Meanwhile, these square patches, being connected horizontally through metal bridges across the slots, carry DC power ( $V_{CC}$  and  $GND$ ) and allow feeding of DC voltages from the left and right borders of the array to the center. Lastly, termination networks (BN in Fig. 1) are inserted to present proper boundary conditions to the peripheral oscillator units (see Section III-D). Since THz

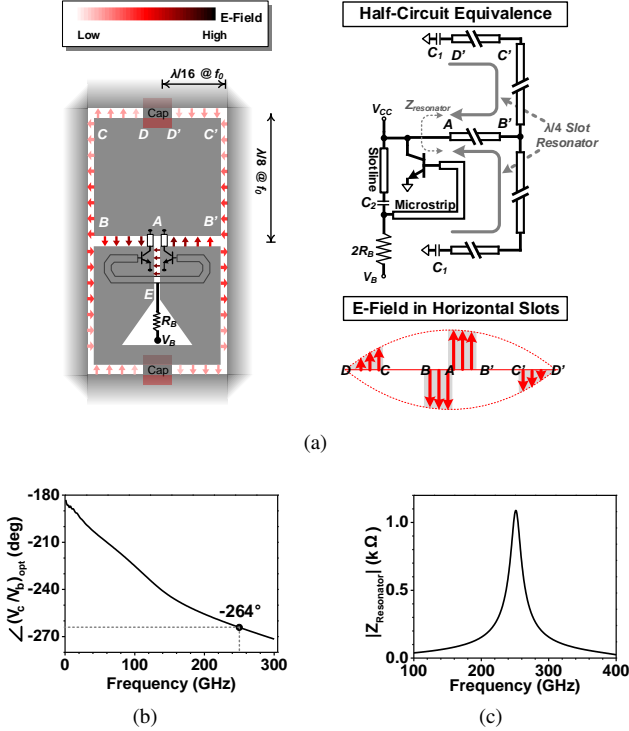


Fig. 2. Operation of a standalone oscillator: (a) field distribution at  $f_0$  and equivalent circuit; (b) simulated optimum transistor phase; (c) simulated resonator impedance presented at Point A.

power is generated in each radiator and there is no need for distribution of centralized input/control signals, this architecture is highly scalable and enables coherent power combining/radiation from a large number of devices.

### III. ENERGY-EFFICIENT 1-THZ RADIATOR DESIGN

The radiator structure is shown in Fig. 1. In this section, we show techniques that exploit the orthogonality of electromagnetic modes and standing-wave geometries to simultaneously optimize oscillation, unit coupling, harmonic generation and radiation slots within one unit. They enable compact circuits and high energy efficiency.

#### A. Fundamental-Frequency Oscillation

To achieve fundamental oscillation at 250 GHz, IHP SiGe HBT process with  $f_{max}$  of 450 GHz is used. Maximizing the device activity requires an optimum phase of device voltage gain to compensate for the intrinsic device delay [5], [6]. To achieve such condition, a pair of differential “self-feeding” oscillators are used. It was previously shown in [5] that with proper impedance and electrical length of the transmission line between the HBT base and collector, the optimum phase condition can be accurately achieved. The half-circuit equivalence of the oscillator is shown in Fig. 2(a). The feedback transmission

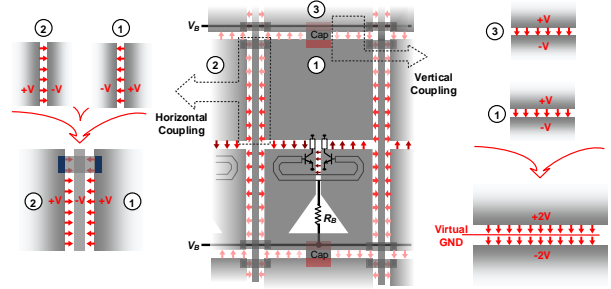


Fig. 3. Horizontal and vertical coupling of adjacent units.

line consists of two sections in series: the first section is a “inverted” microstrip line using M1~M3 layers as signal trace and top metal as ground (Fig. 1(b)), which lowers resistance by removing the vertical via stacks at the HBTs. The second section is a very short Slot  $AE$ , which supports wave propagation of the differential signal at  $f_0$  [5] and isolates the DC bias  $V_B$  and  $V_{CC}$  (modeled as a DC-blocking capacitor  $C_2$  in Fig. 2(a)). In simulation, 40- $\Omega$  impedance and  $34^\circ$  electrical length of the microstrip line achieve the device optimum phase of  $-264^\circ$  (Fig. 2(b)).

For each half of the oscillator, two quarter-wave resonators in shunt are implemented using the horizontal and vertical slots (e.g. Slot  $AB'C'D'$ ). The slots transform the RF short formed by MIM capacitors (see Fig. 1)  $C_1$  into open at Point A, which determines and stabilizes the oscillation frequency. Also note that the near-field radiation at  $f_0$  from each horizontal/vertical slot is canceled by that from the neighboring slot (Fig. 1(a)), leading to a high simulated resonator quality factor  $Q$  of  $\sim 20$  (Fig. 2(c)).

#### B. 2D Synchronization Via Resonator Coupling/Sharing

Strong inter-oscillator coupling is required to minimize the phase difference among units. The four resonators placed at the boundaries of each unit (Fig. 2(a)) make strong coupling possible. Shown in Fig. 3, horizontal coupling (Unit ① and Unit ②) is achieved via close proximity of the vertical slots at the boundaries. Conductor voltages on two sides of one slot are forced to be identical to those of another slot, due to a metal bridge connecting the relevant metal plates. Vertical coupling ((Unit ① and Unit ③)) is achieved by merging the two horizontal slots at the boundaries into one. The two oscillators hence share the same resonator. In both cases above, the high- $Q$  resonators of the adjacent oscillators operate with identical phase and frequency, enabling almost perfect 2D array synchronization without additional power loss and area.

#### C. Efficient Harmonic Generation and Radiation at 1 THz

For maximum 1-THz ( $4f_0$ ) wave generation, radiation at  $2f_0$  and  $3f_0$  should be prevented so that the related power

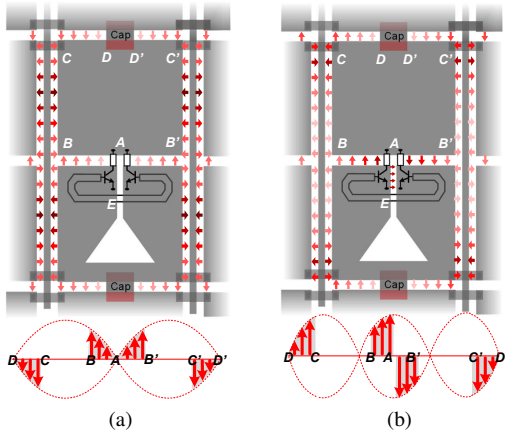


Fig. 4. Wave distribution in the slotlines at (a)  $2f_0$  and (b)  $3f_0$ .

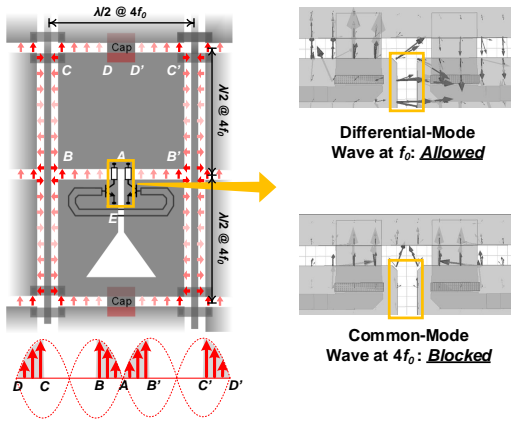


Fig. 5. Wave distribution at  $4f_0$  and mode-filtering simulation of Slot  $AE$  in HFSS (the arrows represent the E-field vectors).

is further up-mixed to  $4f_0$  by the transistors. Similar to that at  $f_0$ , this is achieved again by the standing wave formation in the oscillator slots (Fig. 4). Radiation in all vertical slots is canceled by its out-of-phase counterpart in the horizontally-adjacent oscillator. For the differential-mode signal at  $3f_0$ , radiation cancellation occurs between adjacent horizontal slots (e.g.  $AB$  and  $AB'$ ). For the common-mode signal at  $2f_0$ , waves inside  $AB$  and  $CD$ , as part of the half-wavelength standing wave, are out-of-phase and cancel each other in the near field.

In contrast, for the generated common-mode signal at  $4f_0$ , standing waves formed inside all horizontal slots are in-phase (Fig. 5), resulting in efficient backside radiation ( $\eta_{\text{sim}}=63\%$ ) through an attached silicon lens. On average, each oscillator unit contributes two radiating dipole slots to the array; all these antennas are coherent and optimally separated by  $\lambda_{4f_0}/2$ . For a  $6 \times 7$  array with 91 equivalent slot antennas in total, the simulated directivity is 23.6 dBi. Lastly, we note that the left-right symmetry of the  $4f_0$

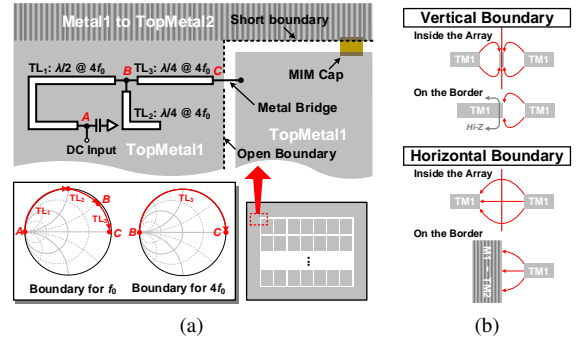


Fig. 6. Array boundary termination: (a) top and (b) cross-sectional views.

signal corresponds to TM mode inside Slot  $AE$ ; unlike the TEM wave of the differential signal at  $f_0$ , its propagation in  $AE$  is not supported due to the slot waveguide cutoff (EM simulation shown in Fig. 5). This isolates the 1-THz signal from lossy HBT bases, increasing the harmonic generation efficiency by approximately a factor of 5.

#### D. Synthesis of the Array Boundary Conditions

For proper array operation, the boundary conditions of the peripheral oscillators should be synthesized to mimic those of the coupled oscillators inside the array. The conditions can be inferred from Fig. 3:

1) *Vertical Boundary*: The slotline pair formed by horizontal coupling essentially comprises a co-planar waveguide, whose center line is open-circuit for electric field (i.e. perfect magnetic conductor boundary). On the left and right sides of the array, this is approximated by a network shown in Fig. 6, which presents open at the two most critical frequencies  $f_0$  and  $4f_0$ , and mimics field that is similar as that inside the array (Fig. 6(b)).

2) *Horizontal Boundary*: The center line of the horizontal boundary slotline behaves as virtual ground (Fig. 3) with short-circuit boundary (i.e. perfect electrical conductor). At the top and bottom side of the array, it is created by a vertical stacked-metal wall (Fig. 6(b)).

## IV. EXPERIMENTAL RESULTS

A  $6 \times 7$  array is fabricated using IHP 130-nm BiCMOS process. The chip occupies  $1\text{-mm}^2$  area and consumes 1.1-W DC power. The output radiation, coupled through a half-ball silicon lens and modulated by a 50%-duty-cycle square wave, is measured at a far-field distance of 3 cm using a WR-1.0 horn antenna and a VDI zero-biased detector (ZBD) with a calibrated responsivity of 1.1 kV/W and NEP of  $57 \text{ pW}/\sqrt{\text{Hz}}$  (Fig. 7(a)). The measured radiation pattern (Fig. 7(b)) has a directivity of 24.0 dBi. A ZBD-received power of  $4 \mu\text{W}$  is obtained from the reading of lock-in amplifier multiplied by  $\pi/\sqrt{2}$  – the ratio between the peak-peak voltage of a square wave and its

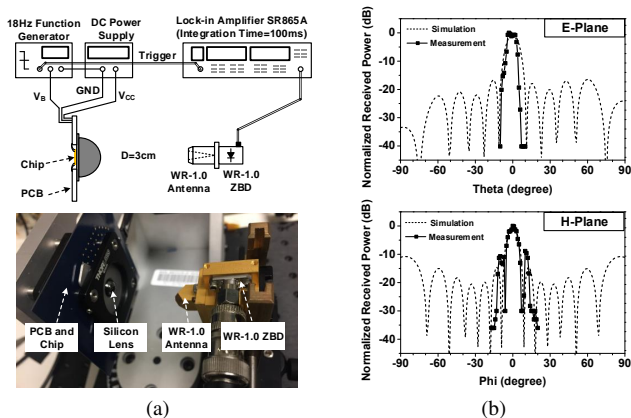


Fig. 7. Measurement using zero-biased diode detector: (a) testing setup and (b) simulated and measured radiation patterns at 1 THz.

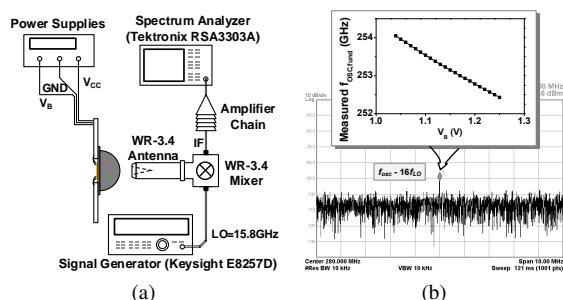


Fig. 8. Fundamental-oscillation frequency ( $f_0$ ) testing: (a) measurement setup, (b) measured spectrum and tuning range.

fundamental-component RMS voltage given by the lock-in amplifier [7]. That results in a total chip-radiated power of -10.9 dBm and EIRP of 13.1 dBm. The output power is also measured using a photo-acoustic TK absolute power meter with large input aperture and lock-in function. By controlling the chip bias  $V_B$ , the radiation is chopped at 30 Hz, which excludes the impact of the slowly-fluctuating heat generated by the chip. The measured radiated power is -10 dBm. The 0.9-dB difference between this and that from the ZBD is likely to be caused by the fundamental-wave leakage that is detectable by the TK power meter but not the ZBD. The leakage may be due to the mismatch of each transistor pair, and its frequency is measured by placing a VDI WR-3.4 subharmonic mixer close to the chip (Fig. 8(a)). With varying base-bias voltage, the measured  $f_0$  changes from 252.4 to 254.0 GHz, corresponding to a tuning range of  $f_{rad}$  from 1.010 THz to 1.016 THz (Fig. 8(b)).

## V. CONCLUSION

Comparisons against previous THz coherent radiators in silicon are presented in Fig. 9 and TABLE I. Using the proposed array architecture, this chip improves the record

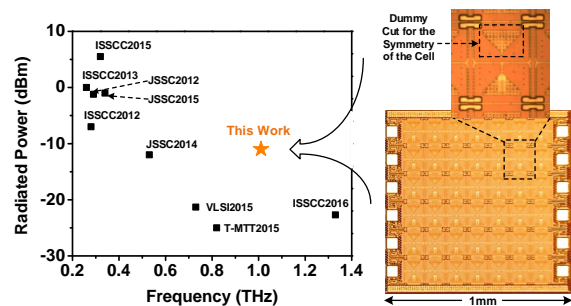


Fig. 9. Die photo and a comparison of Si THz coherent radiators.

TABLE I. COMPARISON OF THZ SOURCES IN SILICON

	This Work	[1]	[2]	[3]	[4]
Type	Oscillating Radiator Array	Antenna-Equipped Frequency Multiplier			
$f_{out}$ (THz)	1.01	0.99	0.82	1.33	0.73
$P_{out}$ (dBm)	-10.9	-37	N/A	-22.7	-21.3
EIRP (dBm)	13.1	N/A	-17	-13	-22.2
$P_{RF,in}$ (dBm)	N/A	8	14	18	13.8
$P_{DC}$ (W)	1.1	4	3.7	0	0
Area (mm <sup>2</sup> )	1.0	3.28	3.22	0.36	0.26
Technology	130-nm SiGe	250-nm SiGe	250-nm SiGe	65-nm CMOS	65-nm CMOS

total radiated power and EIRP in the mid-THz-range (0.6-1.4THz) by 10 dB and 26 dB respectively.

## ACKNOWLEDGMENT

The authors gratefully acknowledge ADI, MIT/MTL GaN Energy Initiative and MIT CICS for funding support, Prof. Qing Hu at MIT for chip testing support, and Dr. Mehmet Kaynak at IHP for chip fabrication support.

## REFERENCES

- [1] K. Statnikov *et al.*, "160-GHz to 1-THz multi-color active imaging with a lens-coupled SiGe HBT chip-set," *IEEE T-MTT*, vol. 63, no. 2, pp. 520-532, 2015.
- [2] E. Öjefors *et al.*, "A 820GHz SiGe chipset for terahertz active imaging applications," *ISSCC*, Feb. 2011.
- [3] Z. Ahmad *et al.*, "1.4THz, -13dBm-EIRP frequency multiplier chain using symmetric- and asymmetric-CV varactors in 65nm CMOS," *ISSCC*, Feb. 2016.
- [4] Z. Ahmad and K. O., "0.65-0.73THz Quintupler with an On-Chip Antenna in 65nm CMOS," *IEEE Symp. VLSI Circuits*, pp. 310311, June 2015.
- [5] R. Han *et al.*, "A SiGe Terahertz Heterodyne Imaging Transmitter with 3.3 mW Radiated Power and Fully-Integrated Phase-Locked Loop," *IEEE JSSC*, vol. 50, no. 12, pp. 2935-2947, 2015.
- [6] O. Momeni *et al.*, "High power terahertz and millimeter-wave oscillator design: a systematic approach," *IEEE JSSC*, vol. 46, no. 3, pp. 583-597, 2011.
- [7] Stanford Research Systems, "SR865A: Operation Manual".